Research Article

Design of a fuzzy PID controller for a MEMS tunable capacitor for noise reduction in a voltage reference source

Ehsan Ranjbar[1] · Mohammad Bagher Menhaj[2] · Amir Abolfazl Suratgar[3] · Javier Andreu-Perez[4] · Mukesh Prasad[5]

Received: 24 November 2020 / Accepted: 15 April 2021
Published online: 06 May 2021

Abstract
This study presents a conventional Ziegler-Nichols (ZN) Proportional Integral Derivative (PID) controller, having reviewed the mathematical modeling of the Micro Electro Mechanical Systems (MEMS) Tunable Capacitors (TCs), and also proposes a fuzzy PID controller which demonstrates a better tracking performance in the presence of measurement noise, in comparison with conventional ZN-based PID controllers. Referring to importance and impact of this research, the proposed controller takes advantage of fuzzy control properties such as robustness against noise. TCs are responsible for regulating the reference voltage when integrated into Alternating Current (AC) Voltage Reference Sources (VRS). Capacitance regulation for tunable capacitors in VRS is carried out by modulating the distance of a movable plate. A successful modulation depends on maintaining the stability around the pull-in point. This distance regulation can be achieved by the proposed controller which guarantees the tracking performance of the movable plate in moving towards the pull-in point, and remaining in this critical position. The simulation results of the tracking performance and capacitance tuning are very promising, subjected to measurement noise.

Article Highlights

- This article deals with MEMS tunable capacitor dynamics and modeling, considering measurement noise.
- It designs and applies fuzzy PID control system for regulating MEMS voltage reference output.
- This paper contributes to robustness increase in pull-in performance of the tunable capacitor.

Keywords Fuzzy PID controller · MEMS · Noise reduction · Tunable capacitor · Voltage reference

1 Introduction

Major principles of Alternating Current (AC) and Direct Current (DC) Micro Electro Mechanical System (MEMS) based Voltage Reference Source (VRS) were first introduced by Suhonen et al. [39] in a plain circuit to produce a fixed voltage. In that work, a tiny parallel-moving plate capacitor was put forth as the basic operational component. Accurate voltage is obtained between the plates of a MEMS Tunable Capacitor (TC) by means of the capacitive

✉ Ehsan Ranjbar, en.ranjbar.eeng@gmail.com | [1]MEMS Dynamics & Control Research Group, Industrial Control Lab, Dept. of Electrical Engineering, Amirkabir University of Technology, Tehran, Iran. [2]Dept. of Electrical Engineering, Amirkabir University of Technology, Tehran, Iran. [3]Dept. of Electrical Engineering, Amirkabir University of Technology, Tehran, Iran. [4]School of Computer Science and Electronic Engineering, University of Essex, Colchester, United Kingdom. [5]School of Computer Science, University of Technology Sydney, Sydney, Australia.

properties of the mechanical stability of a single crystalline silicon. The usage of MEMS TCs have got widespread in electronic circuits due to their cheap cost and micro size. Some previous studies have addressed quality enhancement of the MEMS TC as the most influencing component of voltage reference sources and have developed the VRS to increase their accuracy. Some papers have focused on the micro-machining process of MEMS TCs. They have chiefly proposed an innovative design of micro tunable capacitors and have endeavoured to define the properties of MEMS VRS. Kärkkäinen et al. [23] presented design and characterization of a high stability capacitive MEMS device intended for an AC voltage reference at 100 kHz or higher frequencies. A novel fabrication process was proposed to metallize both surfaces of an electrostatically actuated micro-machined moving plate capacitor to be utilized as an AC voltage reference for electrical metrology purposes. Blard et al. [2] put forth a great-level of stability of voltage references functioning in AC and established upon the pull-in impact in split-fingers MEMS structures. Bounouh et al. [3] developed AC voltage reference ranging from 5 V to 90 V exploiting Epitaxial Silicon On Insulator (SOI) surface micro-machining process. It made precise control of both dimensions and material characteristics feasible. In [4, 5], a novel MEMS structure was proposed which could minimize the impact of leakage capacitances on the stability of the voltage reference and averting compensation of any "built-in voltage" generated at metalsemiconductor interfaces.

Pull-in point is the most significant phenomenon occurring within the MEMS TCs of VRS. The sensitive pull-in point specifies a unique quality which gets back to the electromechanical coupling between the applied electrostatic and spring reaction forces. The basic structure and its operation is illustrated in summary form in Fig. 1a and b [35]. The electrostatic force rises up when the electrical charge on the capacitor plates piles up. Thenceforth, the movable plate is repelled towards the stationary plate close to the threshold region. This region is the point in which the spring force does not endure the electrostatic force and is called the pull-in point. The voltage alteration of the capacitor plates is proportionate to the square of the deflection in the movable plate near the pull-in region. Therefore, the VRS generates a regulated voltage, while its TC is put into work around the pull-in point. At this situation, the MEMS VRS is operated around the pull-in point of its MEMS TC. Some instability is produced by mechanical stress and electrical charge over the dielectric layer, about the pull-in point. Kärkkäinen et al. [22] presented the MEMS AC VRS and affirmed that the charge accumulation of the dielectric layer will drop off if the AC voltage is employed, instead of the DC voltage. In this work, the MEMS AC VRS is the considered mode of operation.

Micro-engineering machinery has progressed in such a way that it is capable of building MEMS TCs with tiny dimensions and dwindled mechanical stress. Nevertheless, the required perpetual stability and sensitive preciseness of the reference voltage value necessitate optimal design and the application of controllers for the MEMS voltage references or TCs. The recent control methods demonstrate that efficient control techniques are employed for MEMS and other mechatronic systems to reduce error and enhance performance: Adaptive Sliding Mode Control (ASMC) with application to MEMS gyroscope [12], control of uncertain systems [29], disturbance rejection control with application to aerospace engineering [40], Artificial Neural Network (ANN) based adaptive control [38] and fuzzy adaptive control [37]. In particular, fuzzy control has gained a lot of interests in performance enhancement for MEMS device drive and operation. Abdel-Hamid et al. [1] exploited an auxiliary fuzzy-based model for predicting the Kalman Filter (KF) positioning error states during Global Positioning System (GPS) signal outages for inertial measurement units (IMU) utilizing MEMS sensors and

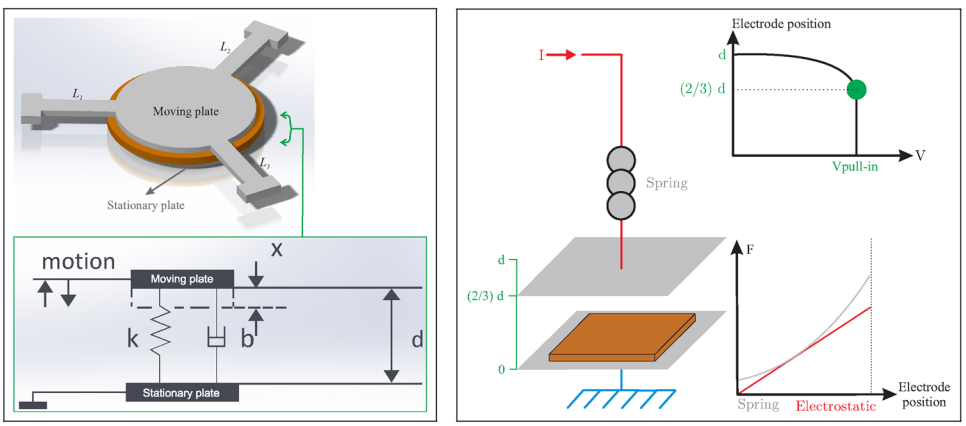

Fig. 1 **a** MEMS tunable capacitor lumped model. **b** Movable plate gets access to one third of its first distance to the fixed plate at the pull-in point [33, 35]

provided corrections to the stand-alone IMU predicted navigation states particularly position. Hong [18] took advantage of fuzzy logic methodology to augment the performance of low cost MEMS gyroscopes. Fei and Xin [15] approached adaptive fuzzy control to estimate the upper bound of the lumped uncertainty in back-stepping Sliding Mode Control (SMC) with application to MEMS triaxial gyroscopes. Approaching optimal control methods, Jeon et al. [20] concentrated over the system-level performance characteristics and surveyed controllers with quadratic optimal control and observed-state feedback control for MEMS-based storage device. The controller damped the oscillations utilizing the actuators and decreased seek time by decreasing settling time. Adopting adaptive and robust control techniques, Rahmani et al. [30] proposed adaptive fractional SMC and robust control-based methods for control of MEMS vibratory gyroscope in presence of external perturbations and model uncertainties. In [31, 32], they have contributed to elimination of the chattering effect and to accuracy increase. Machine learning techniques are also exploited to enhance MEMS device performance. For instance, Zhao et al. [42] employed type-2 sequential fuzzy neural network to suppress the chaotic motion of the MEMS resonator in order to tackle the unknown exogenous disturbance and leave out the impact of time delay in the resonator operation. Associated applications are sometimes expanded. With respect to micro-displacement, such as the micro-positioning in this work, one might specify control methods to drive micro stepper motors. The drive can be set up for Computer Numerical Control (CNC) machining applications capable of precise material removal according to the trajectory of XY positioning stages [26]. Moreover, some of the latest research on adaptive and robust control have addressed modeling deficiencies in MEMS, their parametric uncertainties and disorganized dynamics; some have approached fuzzy algorithms [16, 21] and some have used ANN-based SMC control [41] and others have benefited robust techniques [11, 25].

Mehrnezhad et al. [27] employed a state space model in order to apply various advanced control techniques for MEMS tunable capacitors. Deng et al. [8] established a mathematical model of the pull-in voltage and studied effect factors of manufacturing variations and proposed a control method according to the established model. Some control designs are utilized to push the moving plate against the pull-in region and maintain its stability when the system is prone to parameter uncertainty or gradual alteration such as slow stiffness change in the capacitor's cantilevers. In [34] conventional adaptive control and adaptive SMC were proposed and compared to manage some but not all the mentioned issues in MEMS TC control. Farzanegan et al. [10] proposed Model Reference Adaptive Control (MRAC) for the MEMS TC using output feedback. Ranjbar et al. [33] proposed an observer-based controller for the MEMS TC to cancel the requirement for measurement circuits of displacement and velocity of the movable capacitive plates. Note that the stability of the pull-in easily remains accessible using a straightforward pole-placement state feedback control design. The unavoidable capacitor parametric uncertainties, disturbance and measurement noise, bring up serious challenges, requiring to design more intricate controllers. Impreciseness in the spring and damping factors does not ruin the pull-in stability and plate regulation on its own. The working stability gets worsened when the measurement electrical noise and mechanical noise as well as parameter alteration are considered all together as practical elements affecting capacitor dynamics and performance.

Our challenge in this work is to design a PID controller, which is competent in reducing the measurement noise while fulfilling the main duty of perfect displacement of the MEMS movable capacitive plate towards the pull-in point. The controller simultaneously confronts both noise and disturbance in the dynamics of the MEMS tunable capacitive plates. The movable plate is regulated around the pull-in point while displacing, without provoking destructive motion overshoots. This article contributes to management and rejection of electrical measurement noise, employing a fuzzy PID controller for a MEMS tunable capacitor for the first time. The standard Ziegler-Nichols PID control system is supplanted by a fuzzy PID design in this article. In our tests of the proposed controller, we can conclude that the proposed fuzzy PID design demonstrates a better performance in comparison with the ZN-based PID, owing to more robustness of the fuzzy-structured controllers against noise and disturbance. The measurement noise ruins the read-outs of the displacement and velocity of the movable plate.

The main highlights, contributions and novelties of the work in terms of theoretical developments for this paper can be itemized as follows:

- Unlike previous papers [12, 15, 16] on modeling and control problems of MEMS capacitive plates with sinusoidal oscillations, this article concentrates on smooth displacement of MEMS capacitive plates without any overshoot in a precise micro-meter scale, positioning them near the critical functioning point called the pull-in point when the capacitor dynamics is prone to measurement noise and external disturbance.
- The proposed PID proposes a speedy zero-convergence of the tracking error. Moreover, implementation of the proposed controller can be done via fuzzy tuning of the PID controller parameters without knowing bounds on noise. In the similar previous articles [10, 34], the

convergence-time of the states is longer in comparison with this work. The settling time (convergence) in the proposed controller is also a little shorter (faster) in comparison with [33].

- The proposed FLC has been applied to the MEMS tunable capacitor for voltage regulation for the first time.
- Unlike similar previous works [33, 35] which have used SMC, the proposed method does not suffer from possible excitation of non-modeled modes in the dynamics of the tunable capacitor. This excitation may be brought about by high frequency elements, which are themselves caused by the chattering phenomenon, in the control law enforcing the plate.
- Contrary to earlier articles [33, 36], the designed control law in this article gets applicable to the movable plate in practice because it does not get negative as displayed in simulation results in Sect. 4. In some earlier mentioned papers, the control law also becomes negative which can not be generated in practice because a square of current should produce the control law while being implemented.
- The fuzzy calculation in formation of the control law and the PID coefficients normally results in robustness against disturbance and noise. This paper takes advantage of employment of fuzzy estimators to generate the control law, being superior to earlier non-fuzzy designs from the robustness aspect.
- The proposed fuzzy PID design shows a much better tracking and less energy consumption as a serious replacement with ZN-based PID.
- The manual tuning of the PID controller coefficients is not required because of the automatic fuzzy adjustment of the parameters.

This article is organized as follows: the operation principles and modeling of the MEMS tunable capacitor is presented in Sect. 2. The mathematics for the design of the controller and the preliminaries of the dynamical model are clarified afterwards in Sect. 3. Next, Sect. 4 outlines the performance results. Discussion and conclusion are finally given in Sects. 5 and 6, respectively.

2 MEMS TC operating principles

A tunable capacitor basically encompasses an unmovable plate and a movable one. In our research, a standard tunable capacitor, depicted on Fig. 1a and b [33], is considered. A capacitor is the MEMS parallel plates, including a displaceable plate, which is competent of varying the interplate gap. The plate displacement is appreciably tensed and it is hampered from settling at the pull-in point [34]. In such precise micro positioning application, it is important to ponder the measurement noise in the displacement and velocity of the movable plate of the tunable capacitor to improve the tracking performance of the moving plate, which is charged.

Some models, which are put forth for the TC, demand making assumptions which lead to uncertainty in some parameters. These parameters emerge in the plant dynamics such as stiffness factor and damping coefficient. They transpire as one of the significant characteristics of the movable plate suspension system. Furthermore, device exhaustion and variation in operation condition ruin desired mechanical characteristics, which itself engenders parameter uncertainty. It should not be disregarded that manufacturing procedures themselves originate from uncertainty in the planning of the fabrication procedure and the implementation, which entails uncertainty in the parameters of the fabricated device. For instance, the plate mass, stiffness and damping factors are all subjected to uncertainty in their values. All fabrication procedures are modified so that the resulted uncertainties are slight and inconsiderable. If the uncertainties are slight, ordinary modern controllers are easily capable of passable tracking performance. However, if measurement noise and other exacerbating conditions such as disturbance are also imposed on the system, simple modern controllers will be hampered in achieving effective performance. Main parameters of the MEMS tunable capacitor are presented in Table 1.

MEMS tunable capacitance is equal to:

$$C = \epsilon A/(d - x)\,. \tag{1}$$

The parameters in Eq. (1), including ε, d, x and A, are permittivity, initial distance between the plates, movable plate displacement and plate area. Actuation of the capacitor is carried out by an AC current given by Eq. (2);

$$I = I_m \sin(\omega t)\,. \tag{2}$$

Electrodes are attracted towards each other by the electrostatic force which is denoted by F_E. Spring force, which is equal to kx, hampers plates from getting close to each other. These two forces are expressed by Eq. (3) regarding Fig. 1a [6, 24];

$$F_E = |-\frac{\partial E_I}{\partial x}| = \frac{I_m^2 \cos^2(\omega t)}{2\epsilon A\omega^2} = kx + b\frac{\mathrm{d}x}{\mathrm{d}t} + m\frac{\mathrm{d}^2x}{\mathrm{d}t^2}\,. \tag{3}$$

Table 1 Modeling parameters of the MEMS tunable capacitor

Parameter	Real value	Parameter	Real value
m	1.11×10^{-7} Kg	k	2338 N/m
b	0.01 Ns/m	d	2 μm

The parameters of Eq. (3), including F_E, E_I, x, k, m and b, are respectively the electrostatic force, electrostatic energy, plate distance, spring constant, movable mass, and damping factor. f_{ac}, which is the current alternating frequency, is defined by Eq. (4) and plays the actuation role;

$$f_{ac} = \omega/2\pi\,. \tag{4}$$

The other frequency, which should be taken into account, is the mechanical resonance frequency and is given by Eq. (5);

$$f_m = \omega_0/2\pi = \sqrt{k/m}/2\pi\,. \tag{5}$$

f_m is considered to be much smaller than f_{ac} because we can opt for higher values for f_{ac}. The pull-in point is the damping region for the extra displacement of the movable plate and is known as the stability point. The gas trapped inside the device package is the chief damper resisting against the movable plate displacement. In Eq. (3), damping is symbolized by b. In the steady state, the position of the movable electrode is nearly assumed to be constant. Consequently, plate velocity and acceleration, symbolized by $\dot{x}$ and $\ddot{x}$ respectively, converge to zero. Considering the plate mechanical behaviour, the electrostatic coercion in Eq. (3) is replaced by its mean value, yielding Eq. (6) around the operational pull-in point. The consequent mathematical re-presentation is given below:

$$\bar{F}_E = \frac{2}{T}\int_0^{\frac{T}{2}} \frac{I_m^2\cos^2(\omega t)}{2\epsilon A\omega^2}\mathrm{d}t = \frac{1}{\pi}\int_0^{\pi} \frac{I_m^2(1+\cos(2\alpha))}{4\epsilon A\omega^2}\mathrm{d}\alpha = \frac{I_{RMS}^2}{2\epsilon A\omega^2\pi} = kx\,. \tag{6}$$

The electrostatic force, which moves the plate, is re-expressed in terms of the AC voltage Root Mean Square (RMS) value by the subsequent equation,

$$\bar{F}_E = |-\frac{\partial E_V}{\partial x}| = \frac{\epsilon A V_{RMS}^2}{2(d-x)^2} = kx\,. \tag{7}$$

V_{RMS} symbolizes the RMS voltage between the plates and E_V stands for the electrostatic energy. Let us express x in terms of I_{RMS} from Eq. (6). Then, replace x in Eq. (7) with the pervious result. It leads to achievement of Eq. (8). Consequently, V_{RMS} is achieved in terms of I_{RMS} [27]. They are all mathematically stated in the following expressions:

$$V_{RMS} = \frac{d}{\epsilon A\omega} I_{RMS} - \frac{1}{2k\epsilon^2 A^2\omega^3} I_{RMS}^3\,. \tag{8}$$

Derivative of V_{RMS} with respect to I_{RMS} leads to Eq. (9);

$$\frac{\partial V_{RMS}}{\partial I_{RMS}} = \frac{d}{\epsilon A\omega} - \frac{3}{2k\epsilon^2 A^2\omega^3} I_{RMS}^2\,. \tag{9}$$

Putting Eq. (9) equal to zero gives the respective maximum value for the RMS AC current;

$$I_{RMS}^{max} = \sqrt{2kd\epsilon A\omega^2/3}\,. \tag{10}$$

In order to achieve the respective maximum value of the RMS AC voltage, I_{RMS} in Eq. (8) should be supplanted with the previous obtained value of the maximum RMS AC current. Thenceforth, the pull-in voltage, which is denoted by V_{RMS}^{max}, is given by the following expression;

$$V_{RMS}^{max} = \sqrt{8kd^2/27C_0} = \sqrt{8kd^3/27\epsilon A}\,. \tag{11}$$

Combining Eqs. (6) and (7), the plate displacement, x, is calculated with regard to Eq. (12). It is equal to

$$x = d/3\,. \tag{12}$$

Note that the attained maximum V_{RMS}^{max} and its respective value I_{RMS}^{max} are employed to achieve Eq. (12) [27].

Some partial variations in the input current about the pull-in operational point has influence over the output voltage characteristics. That is the reason we need to study the current variation more profoundly. This is the rationale behind Eq. (8) as Eq. (13), assuming ΔI to be the current alteration;

$$\Delta V = \frac{d\Delta I}{\epsilon A\omega} - \frac{(\Delta I^3 + 3I_{RMS}^{max\,2}\Delta I + 3I_{RMS}^{max}\Delta I^2)}{2k\epsilon^2 A^2\omega^3}\,. \tag{13}$$

Division of Eq. (13) by the maximum value of RMS AC voltage brings about Equation (14);

$$\frac{\Delta V_{RMS}}{V_{RMS}^{max}} = -\frac{3}{2}\left(\frac{\Delta I}{I_{RMS}^{max}}\right)^2 - \frac{1}{2}\left(\frac{\Delta I}{I_{RMS}^{max}}\right)^3 \approx -\frac{3}{2}\left(\frac{\Delta I}{I_{RMS}^{max}}\right)^2\,. \tag{14}$$

Equation (14) states that the voltage changes in the pull-in region is nearly proportional to the square of the current alteration. Consequently, tiny partial changes in the input current cause a tiny change in the pull-in voltage. It backs the idea of the usage of the tunable capacitors as the chief components in a VRS circuitry. If f_{ac} is set in such a way that it is much bigger than the mechanical frequency f_m, the electrostatic force in Eq. (3) can be replaced by the mean value of the electrostatic force. It yields Eq. (15);

$$\bar{F}_E = \frac{I_{RMS}^2}{2\epsilon A\omega^2\pi} = u = m\ddot{x}(t) + b\dot{x}(t) + kx(t)\,. \tag{15}$$

At the end of this section, we would explicitly add up the assumptions and constraints, which were exploited in our modeling, as follows:

- It is assumed that the frequency of the electrical actuation $\left(f_{ac} = \omega/2\pi\right)$ is much bigger than the resonance frequency of the described resonator system of the MEMS tunable capacitor. This makes the tunable capacitor respond to just the average of the electro-

static force. Otherwise, it may respond in an oscillatory manner which is not our desired capacitive movement.
- It is assumed that the deviation of the physical parameters of the MEMS tunable capacitor, including the plate mass, stiffness factor, and damping coefficient, from the nominal values is negligible.
- The tunable capacitor takes advantage of geometrical symmetry.
- It is supposed that the MEMS tunable capacitor will be put in a package in which damping gas is entrapped.
- It is presumed that the squeeze film damping is the dominant damping effect and the slide film damping is inconsiderable.
- The suspension system of the movable plate constrains the movable plate to get displaced just along one direction (x axis). Not only does this chiefly eliminate the slide film damping effect, but also it prevents cross-talk end emergence of cross damping factors and cross stiffness coefficients such as d_{xy}, k_{xy}, etc.
- The reference model, adopted by the designer, constrains the system to show a critically damped behaviour.
- The voltage alterations in the pull-in point is approximately proportional to the square of the current changes.

3 Control design and simulation

Applying Laplace transform to Eq. (15), the plant input-to-output dynamics can be described by the following equation:

$$G_p(s) = \frac{X(s)}{U(s)} = \frac{K}{b_2 s^2 + b_1 s + b_0}, \tag{16}$$

where $K = 9.009e06$, $b_2 = 1$, $b_1 = 9.009e04$ and $b_0 = 2.106e10$. The poles of the plant are:

$$s_{1,2} = -45045.045 \pm j1379.638. \tag{17}$$

The root-locus for $G_p(s)$ is depicted in Fig. 2a. In one of the methods for designing a PID with the Ziegler-Nichols table, the designer needs to put the system into oscillation via an appropriate gain. This gain (K_u) and the corresponding oscillation period (T_u) are the tuning/schedualing design factors in Table 2. For this purpose, a pole is added to the plant to have asymptotes with degrees of 60°, −60° and 180° in the modified system of $G_{tot}(s)$, considering Eq. (18) for the angles of the root locus asymptotes [9]. The asymptote angle equation is:

$$\phi = \frac{(2w+1)180^\circ}{n_z - m_z} \quad (w = 0, 1, \ldots, n_z - m_z - 1), \tag{18}$$

where n_z and m_z respectively symbolize the degrees of the denominator and nominator of $G_{tot}(s)$. The modified plant is

$$G_{tot}(s) = G_{c_1}(s) G_p(s), \tag{19}$$

where

$$G_{c_1}(s) = \frac{K_{c_1}}{(s + c_1)} = \frac{1}{s + 8000}. \tag{20}$$

Putting Eqs. (19), (20), and (16) together yields

$$G_{tot}(s) = \frac{K_{c_1} K}{(s + c_1)(b_2 s^2 + b_1 s + b_0)}. \tag{21}$$

The Routh-Hurwitz test is a mathematical criterion which is a necessary and sufficient condition for testing the stability of a linear time invariant (LTI) system. Our system Routh-Hurwitz table is obtained as:

$$\begin{array}{c|cc} s^3 & b_2 & c_1 b_1 + b_0 \\ s^2 & b_1 + c_1 b_2 & c_1 b_0 + K_{c_1} K \\ s & t_{32} & \\ s^0 & c_1 b_0 + K_{c_1} K & \end{array} \tag{22}$$

where

$$t_{32} = \frac{(b_1 + c_1 b_2)(c_1 b_1 + b_0) - b_2 (c_1 b_0 + K_{c_1} K)}{b_1 + c_1 b_2}. \tag{23}$$

The auxiliary polynomial is:

$$A(s) = (b_1 + c_1 b_2) s^2 + c_1 b_0 + K_{c_1} K. \tag{24}$$

The value for K_{c_1}, which makes the row after the auxiliary polynomial row zero, is equal to

$$K_{c_1} = \frac{-c_1 b_0 b_2 + (b_1 + c_1 b_2)(c_1 b_1 + b_0)}{K b_2}, \tag{25}$$

which leads to the following oscillation (marginal stability) period;

$$T_u = 2\pi / \sqrt{\frac{c_1 b_0 + K_{c_1} K}{b_1 + c_1 b_2}}. \tag{26}$$

K_u and T_u are respectively equal to 2184778.378 and 42.571 μSec. The controller in Fig. 3a has the following equation:

$$G_c(s) = K_p + \frac{K_i}{s} + \frac{K_d}{s} = K_p \left(1 + \frac{1}{T_i s} + T_d s\right), \tag{27}$$

where K_p, K_i and K_d are the PID coefficients in such a way that $K_i = K_p / T_i$ and $K_d = K_p T_d$.

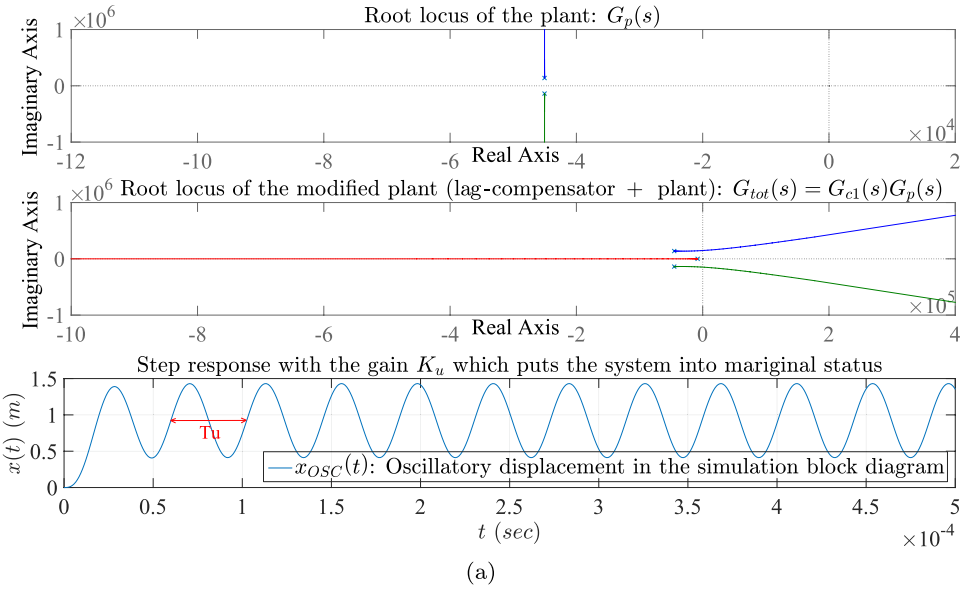

Fig. 2 **a** Root locus of $G_p(s)$ as well as $G_{tot}(s)$, and K_u calculation; K_u is determined so that the system, $G_{tot}(s)$, responds in an oscillatory manner. **b** Block diagram for testing K_u effect on the system response

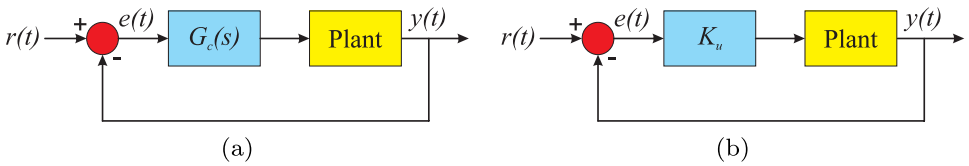

Fig. 3 **a** The PID controller is placed in a unit negative feedback loop. **b** The gain K_u is defined so that the system responds to the step input in an oscillatory manner. The obtained K_u is one of the scheduling factors for the PID design based on the Ziegler-Nichols method

Table 2 The Ziegler-Nichols method for determination of the PID controller coefficients

Controller type	K_p	K_i	K_d
P	$0.5K_u$	–	–
PI	$0.45K_u$	$1.2K_p/T_u$	–
PD	$0.8K_u$	–	$K_pT_u/8$
PID	$0.6K_u$	$2K_p/T_u$	$K_pT_u/8$

In the Ziegler-Nichols method and our design approach, the modified plant is considered as G_{tot} without K_u. Then, the coefficients are determined according to Table 2. The design factors in this table are K_u and T_u. The former is the static gain which puts the plant into marginal status in Fig 3b, making the response an oscillatory one. T_u is the oscillation period. Also, the designer has the freedom to modulate the controller according to the aforementioned table. It is common to use the design set of $\{K_p, K_d, \alpha\}$ instead of $\{K_p, K_d, K_i\}$ where

$$K_i = K_p^2/\alpha K_d \ , \ \alpha = T_i/T_d \, . \tag{28}$$

Normally, $2 \leq \alpha \leq 5$ and for the Ziegler-Nichols α is adopted equal to 4.

In contrast, in a fuzzy PID, the set of $\{K_p, K_d, \alpha\}$ is tuned via a Fuzzy Inference System (FIS). The FIS gets the tracking error, $e(t)$, and its time-derivative, $\dot{e}(t)$, as the inputs and gives the controller parameters including $\{K'_p, K'_d, \alpha\}$ as the outputs. See Fig. 4b. Note that the outputs, $\{K'_p, K'_d\}$, are the normalized values of the main set of $\{K_p, K_d\}$ just for

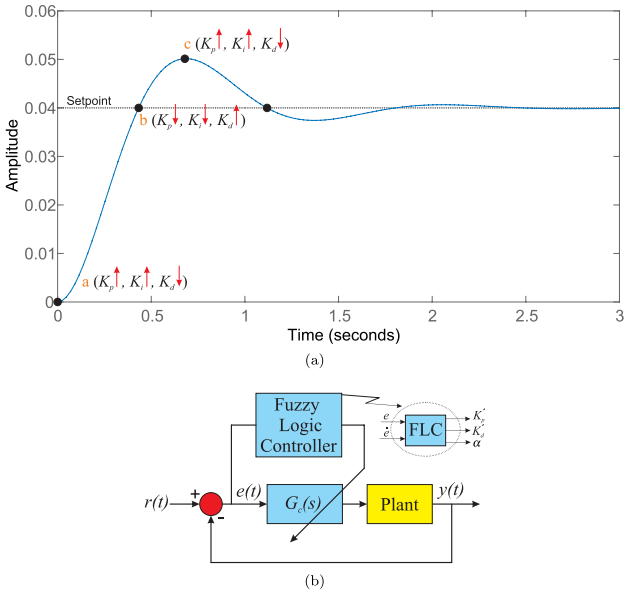

Fig. 4 **a**. Determination of variation of the PID coefficients with respect to the tracking error and its time-derivative. **b** The Fuzzy Logic Controller (FLC) is an FIS which determines the set of $\{K'_p, K'_d, \alpha\}$ or $\{K_p, K_d, \alpha\}$ given the tracking error and its time-derivative

simplicity of working with the values $\in [0, 1]$. The following equations correlate the new set of the controller parameters and the previous one:

$$K'_p = \left(K_p - K_p^{min}\right) / \left(K_p^{max} - K_p^{min}\right), \tag{29}$$

$$K'_d = \left(K_d - K_d^{min}\right) / \left(K_d^{max} - K_d^{min}\right), \tag{30}$$

where K_p^{min}, K_p^{max}, K_d^{min} and K_d^{max} are obtained by the conventional empirical relations:

$$K_p^{min} = 0.32K_u \ , \ K_p^{max} = 0.6K_u \tag{31}$$

$$K_d^{min} = 0.08K_uT_u \ , \ K_d^{max} = 0.15K_uT_u \, . \tag{32}$$

Figure 4a illustrates the working principle of a fuzzy PID logic controller [43]. The PID coefficients are varied by the controller according to the tracking error and its derivative. Some critical points are displayed in this figure, which reveals the manipulation of the coefficients of the controller according to the fuzzy rules. Tables 3, 4 and 5 present the rules for determination of K'_p, K'_d and α. The FIS structure, which is shown in Fig. 5, describes the data flow from the Input $(e, \dot{e})$ to the Output $\left(K'_p, K'_d, \alpha\right)$. First off, the inputs, are fuzzified via two sets of linguistic variables as follows:

$$A = \{Negative\ Large\ (NL), Negative\ Medium\ (NM), Negative\ Small\ (NS), Zero\ (Z), Positive\ Small\ (PS), Positive\ Medium\ (PM), Positive\ Large\ (PL)\}\,. \tag{33}$$

As seen in Fig. 6b, there are 7 linguistic variables for each input; e and $\dot{e}$. Seven membership degrees, between 0 and 1, are allocated to each value of the error and its time-derivative in correspondence with the seven mentioned linguistic variables. They are triangular and trapezoid membership functions. For the first and second outputs, including K'_p and K'_d, there are two linguistic variables;

$$B = \{Small, Large\}, \tag{34}$$

which are displayed in Fig. 6c. For the third output, α, there are also four crisp values;

$$C = \{2, 3, 4, 5\} \tag{35}$$

They are also observable in Fig. 6c. The membership function, which specifies how much e belongs to each member of A, is $\mu_{A_i}(e)$ for i^{th} rule in Tables 3, 4 and 5. The membership function, which determines how much $\dot{e}$ belongs to each member of A, is also $\mu_{A_i}(\dot{e})$ for i^{th} rule in Table 3, 4 and 5. As displayed in Fig. 5, the fuzzified input is now given to the fuzzy rule base whose duty is specification of the membership values for each of the three outputs. Two membership functions, in association with $x = K'_p$ and $x = K'_d$, are described by the following equations:

$$\mu_{B\{Small\}}(x) = \min\left(-\frac{1}{4}\ln(x), 1\right) \tag{36}$$

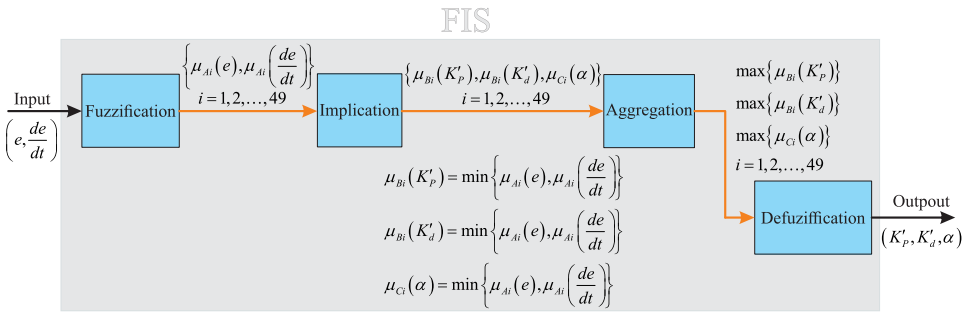

Fig. 5 FIS structure of the fuzzy controller as a mapping from the input to the output

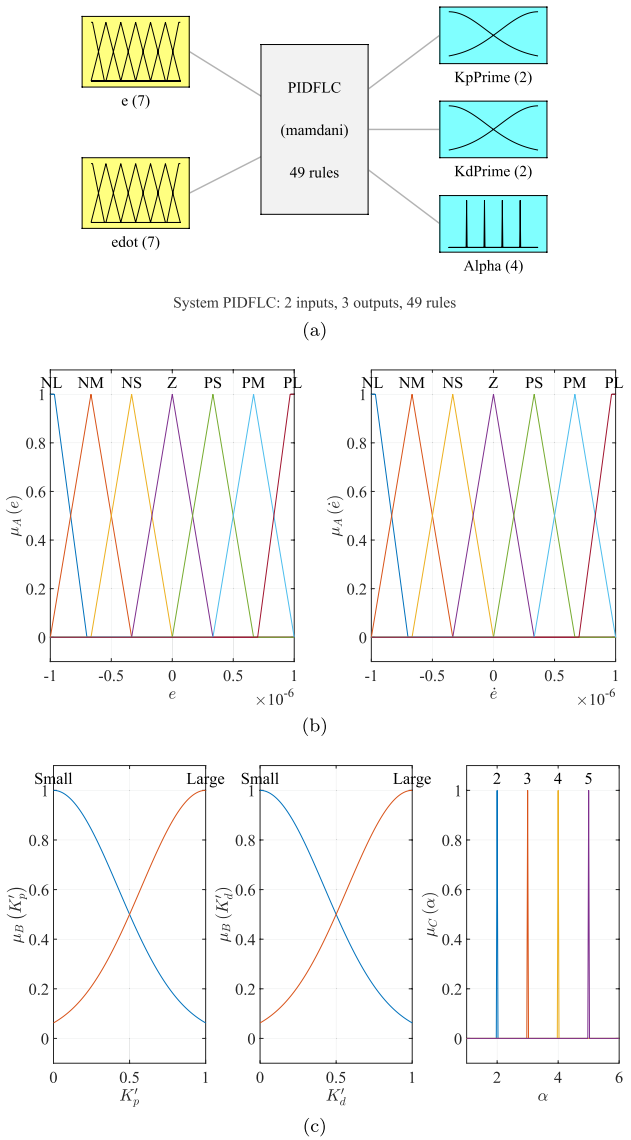

Fig. 6 **a** FIS structure functions as a fuzzy inference engine to map the inputs to the output space. **b** Input triangular and trapezoid membership functions with respect to seven linguistic variables of the set *A*. **c** Two output membership functions are adopted with respect to two linguistic variables of the set *B* and the third group of the membership functions are considered regarding four linguistic variables of the set *C*

$$\mu_{B\{Large\}}(x) = \min\left(-\frac{1}{4}\ln(1-x), 1\right) \tag{37}$$

The third output membership function, in association with α, are very narrow triangular functions resembling singleton membership functions. The implication output are $\mu_{B_i}\left(K'_p\right)$, $\mu_{B_i}\left(K'_d\right)$, and $\mu_{C_i}(\alpha)$, for the i^{th} rule in Tables 3, 4 and 5, respectively. This calculation is done via the following equations:

$$\mu_{B_i}\left(K'_p\right) = \min_{\substack{i=1,2,\ldots,49 \\ \text{for} i^{th} \text{rule in Table3}}} \left\{\mu_{A_i}(e), \mu_{A_i}(\dot{e})\right\}, \tag{38}$$

$$\mu_{B_i}\left(K'_d\right) = \min_{\substack{i=1,2,\ldots,49 \\ \text{for} i^{th} \text{rule in Table 4}}} \left\{\mu_{A_i}(e), \mu_{A_i}(\dot{e})\right\}, \tag{39}$$

$$\mu_{C_i}(\alpha) = \min_{\substack{i=1,2,\ldots,49 \\ \text{for} i^{th} \text{rule in Table 5}}} \left\{\mu_{A_i}(e), \mu_{A_i}(\dot{e})\right\}. \tag{40}$$

The calculated membership degrees, including $\mu_{B_i}\left(K'_p\right)$, $\mu_{B_i}\left(K'_d\right)$ and $\mu_{C_i}(\alpha)$, respectively represent the fuzzy input values of K'_p, K'_d and α for the i^{th} rule in Tables 3, 4 and 5. Actually, the horizontal line with the height equal to either values of Eqs (38), (39) or (40) intersects the corresponding output membership function related to the i^{th} rule in Fig 6c. The respective values of K'_p, K'_d, and α, under the cut of the each of the output membership function in that figure and related to the i^{th} rule, are the values all in our interest. As a matter of fact, they are the weights for each i^{th} rule. The cuts are aggregated using an AND operator. It calculates the maximum of $\mu_{B_i}\left(K'_p\right)$, $\mu_{B_i}\left(K'_d\right)$ and $\mu_{C_i}(\alpha)$ for each value of K'_p, K'_d and α, independently and respectively, for all the rules;

$$f_1\left(K'_p\right) = \max_{i=1,2,\ldots,49} \mu_{B_i}\left(K'_p\right), \ \left(\text{for} \forall K'_p \in [0 \ \ 1]\right), \tag{41}$$

$$f_2\left(K'_d\right) = \max_{i=1,2,\ldots,49} \mu_{B_i}\left(K'_d\right), \ \left(\text{for} \forall K'_d \in [0 \ \ 1]\right), \tag{42}$$

Table 3 The fuzzy rule base for determination of K'_p

$\dot{e}$		NL	NM	NS	Z	PS	PM	PL
e	NL	Large	Large	Large	Large	Large	Large	Large
	NM	Small	Large	Large	Large	Large	Large	Small
	NS	Small	Small	Large	Large	Large	Small	Small
	Z	Small	Small	Small	Large	Small	Small	Small
	PS	Small	Small	Large	Large	Large	Small	Small
	PM	Small	Large	Large	Large	Large	Large	Small
	PL	Large	Large	Large	Large	Large	Large	Large

Table 4 The fuzzy rule base for determination of K'_d

$\dot{e}$		NL	NM	NS	Z	PS	PM	PL
e	NL	Small	Small	Small	Small	Small	Small	Small
	NM	Large	Large	Small	Small	Small	Large	Large
	NS	Large	Large	Large	Small	Large	Large	Large
	Z	Large	Large	Large	Large	Large	Large	Large
	PS	Large	Large	Large	Small	Large	Large	Large
	PM	Large	Large	Small	Small	Small	Large	Large
	PL	Small	Small	Small	Small	Small	Small	Small

Table 5 The fuzzy rule base for determination of α

$\dot{e}$		NL	NM	NS	Z	PS	PM	PL
e	*NL*	2	2	2	2	2	2	2
	NM	3	3	2	2	2	3	3
	NS	4	3	3	2	3	3	4
	Z	5	4	3	3	3	4	5
	S	4	3	3	2	3	3	4
	PM	3	3	2	2	2	3	3
	PL	2	2	2	2	2	2	2

$$f_3(\alpha) = \max_{i=1,2,\ldots,49} \mu_{C_i}(\alpha)\ ,\ (\text{for } \forall\alpha \in [1\ \ 6]). \tag{43}$$

The rule firing strengths, including f_1, f_2 and f_3, are given to the defuzzification subsystem. Bisector method and f_js for $j = 1, 2, 3$, are employed for calculating K'_{pbs}, K'_{dbs}, and α_{bs} with respect to the given e and $\dot{e}$:

$$\int_{-\infty}^{K'_{pbs}} f_1\left(K'_p\right)\mathrm{d}K'_p = \int_{K'_{pbs}}^{\infty} f_1\left(K'_p\right)\mathrm{d}K'_p, \tag{44}$$

$$\int_{-\infty}^{K'_{dbs}} f_2\left(K'_d\right)\mathrm{d}K'_d = \int_{K'_{dbs}}^{\infty} f_2\left(K'_d\right)\mathrm{d}K'_d, \tag{45}$$

$$\int_{-\infty}^{\alpha_{bs}} f_3(\alpha)\mathrm{d}\alpha = \int_{\alpha_{bs}}^{\infty} f_3(\alpha)\mathrm{d}\alpha. \tag{46}$$

It makes no considerable difference in simulation results if they are obtained by centroid method;

$$K'_{pc} = \frac{\int_{-\infty}^{\infty} f_1\left(K'_p\right)K'_p\mathrm{d}K'_p}{\int_{\infty}^{\infty} f_1\left(K'_p\right)\mathrm{d}K'_p}, \tag{47}$$

$$K'_{dc} = \frac{\int_{-\infty}^{\infty} f_1\left(K'_d\right)K'_d\mathrm{d}K'_d}{\int_{-\infty}^{\infty} f_1\left(K'_d\right)\mathrm{d}K'_d}, \tag{48}$$

$$\alpha_c = \frac{\int_{-\infty}^{\infty} f_3(\alpha)\alpha\mathrm{d}\alpha}{\int_{-\infty}^{\infty} f_3(\alpha)\mathrm{d}\alpha}. \tag{49}$$

Set of either $\{K'_{pbs}, K'_{dbs}, \alpha'_{bs}\}$ or $\{K'_{pc}, K'_{dc}, \alpha'_c\}$ are adopted to calculate $\{K'_p, K'_d, \alpha\}$, and $\{K_p, K_d, K_i\}$ for the final PID tuning (Fig. 7).

4 Results and comparison study

The simulation block diagram for the fuzzy PID controller is given in Fig. 8. The simulation block diagram for the Ziegler-Nichols (ZN) based PID with G_{c_1} is also depicted in Fig. 9a while ZN-based without G_{c_1} is displayed in Fig. 9b. A measurement random noise is imposed on the system while measuring the displacement state of the movable plate. Figure 10 illustrates a comparison for the tracking performance for the two types of controller. The blue curve related to the displacement caused by the fuzzy PID controller has less perturbation from the desired trajectory (red curve) in comparison with the green curve which belongs to the Ziegler-Nichols PID controller. Figure 11a independently looks over the tracking error in a magnified manner and approves the aforementioned claim. Figure 11b, from left to right, illustrates the error histogram for the fuzzy PID, ZN PID with pre-compensator of G_{c_1} and ZN PID without G_{c_1}. It demonstrates the improved tracking

performance of the designed fuzzy PID controller, in the presence of displacement measurement noise. Figure 11c also depicts the unacceptable performance of the ZN PID without the pre-compensator in noisy conditions. The proposed fuzzy PID has shown an adequate performance in tracking the desired pull-in trajectory for moving the capacitive plate. It has also outperformed the conventional ZN PID with respect to energy consumption. Figure 12a displays less control effort needed in the proposed fuzzy PID in comparison to the ZN PID controller. The advantages of the proposed FIS control scheme owe to soft variation and tuning of the PID coefficients, as depicted in Fig. 12b.

Comparing our results with some recent published work and showing clearly how the new design features in the current work, we would mention some comparative points as follows. Unlike previous papers on modeling and control problems of MEMS capacitive plates with sinusoidal oscillations such as [7, 13, 14, 17, 19], this

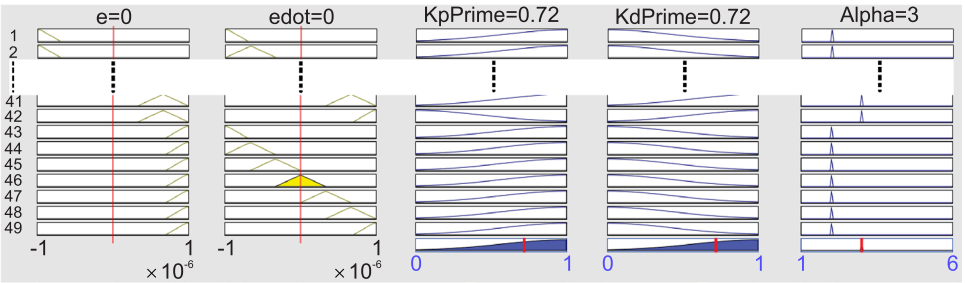

Fig. 7 The red lines are the bisector lines showing the final values for K'_{pbs}, K'_{dbs}, and α_{bs}

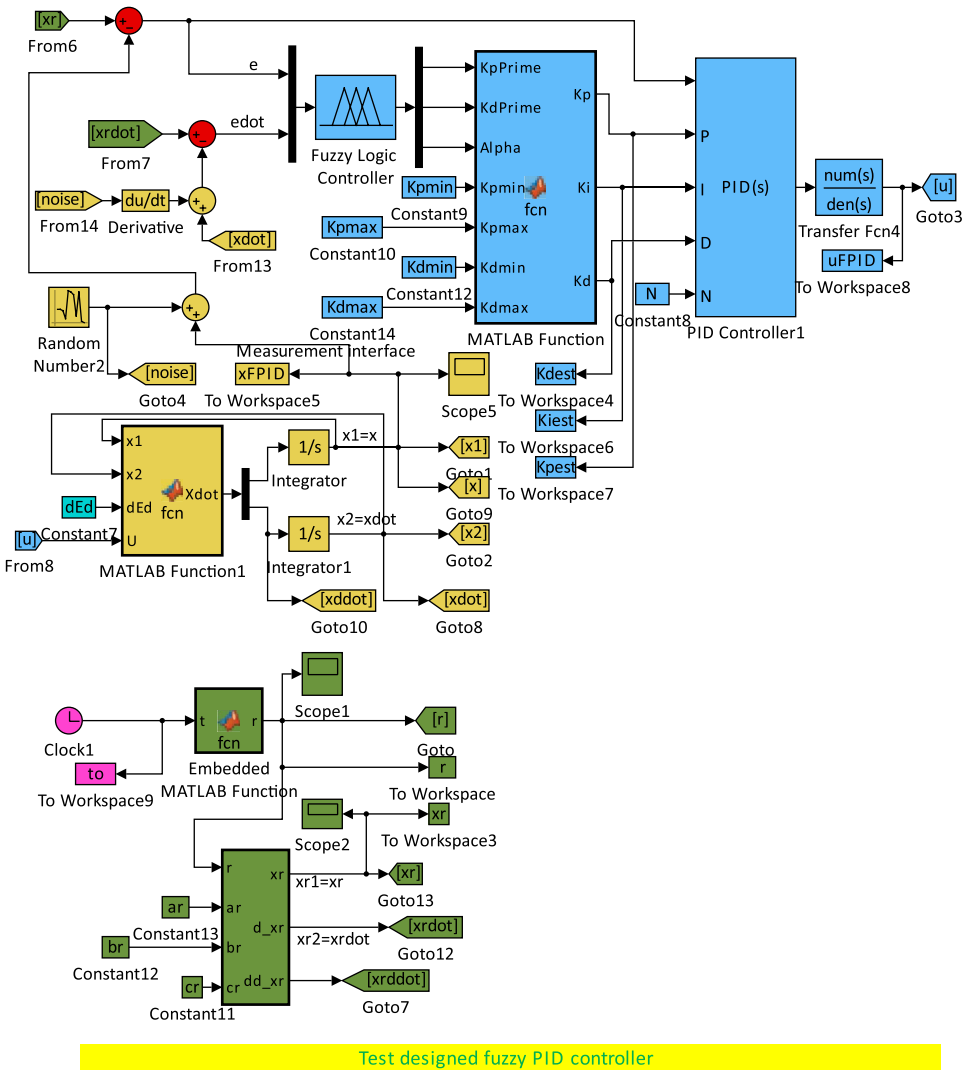

Fig. 8 Simulation block diagram of the fuzzy PID controller for the distance adjustment of the MEMS tunable capacitor plate

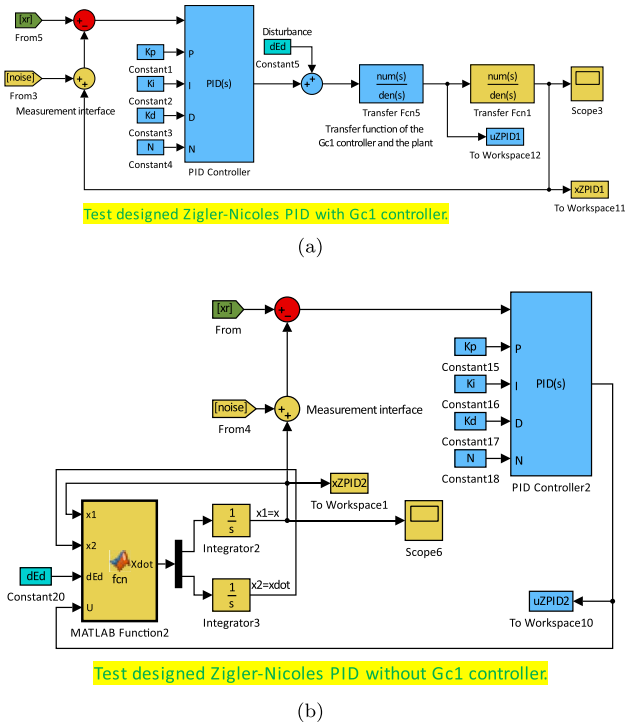

Fig. 9 **a** Simulation block diagram for the Ziegler-Nichols (ZN) based PID with G_{c_1}. **b** The simulation block diagram for the ZN based PID without G_{c_1} *pre-compensator*

article presents solution for displacing MEMS capacitive plates smoothly without any overshoot in a precise micro-meter scale, and for positioning them adjacent to the pull-in point, subjected into measurement noise and external disturbance. The proposed PID demonstrates a faster zero-convergence of the tracking error in comparison to [10, 28, 34]. In comparison with [33], the settling time in the proposed control system is also a little shorter. Comparing this work with [10, 33–36] which are based on SMC to enrich the robustness and suffer the chattering

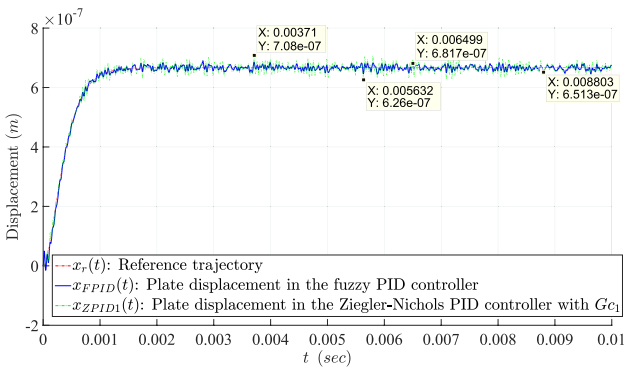

Fig. 10 Comparison of the tracking performance between the fuzzy and Ziegler-Nichols PIDs

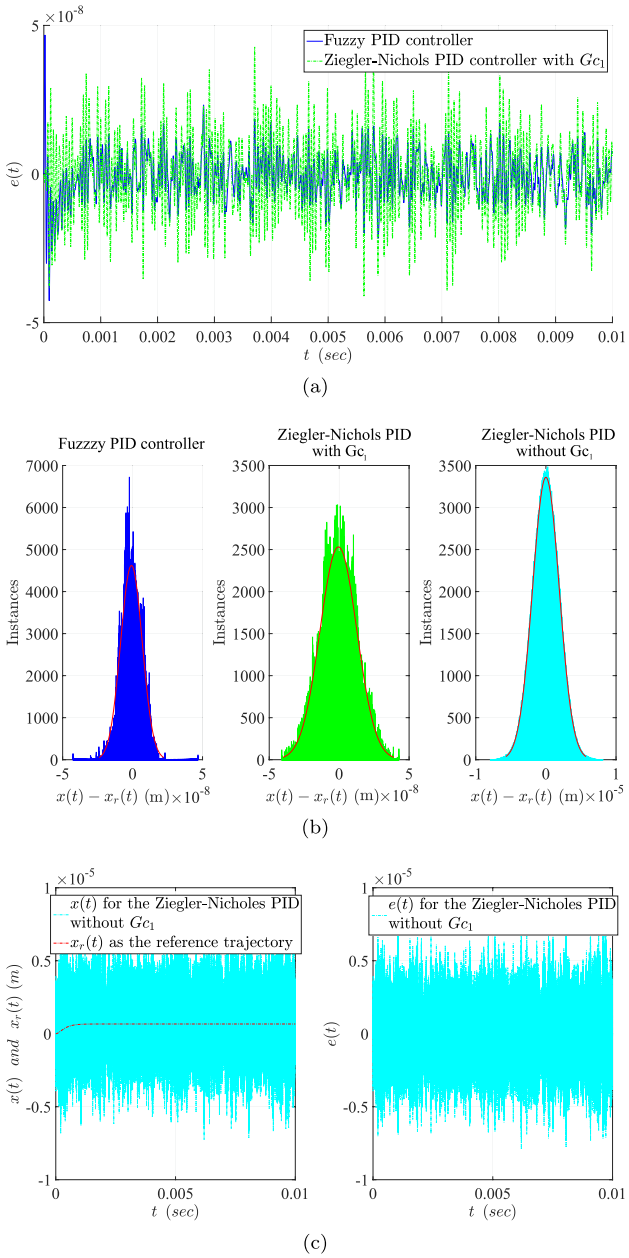

Fig. 11 **a** Comparison of the tracking error between the fuzzy and Ziegler-Nichols PIDs. **b** Tracking error histograms of the fuzzy PID, ZN PID with pre-compensator of G_{c_1} and ZN PID without G_{c_1}. **c** Tracking performance and error for the ZN PID without G_{c_1}

phenomenon, the proposed control system is alleviated of excitation of un-modeled modes in the dynamics of the capacitor due to smooth fuzzy tuning of the coefficients constructing the control law. As displayed in [34] on modal analysis (Page 12 - Fig. 8 in that paper), the high frequency elements can result in the plate deformation and undesired capacitance. Contrary to previous articles [33–36], the proposed control effort in this paper can be applied to the displaceable plate in practice because it

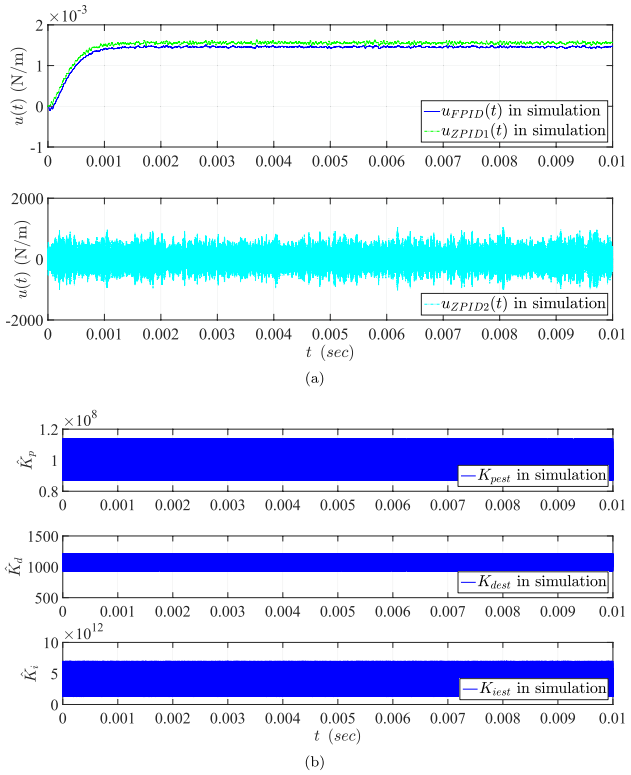

Fig. 12 **a** Less control effort of the fuzzy PID controller in comparison to the ZN PID. **b** Tuning of the PID coefficients by the FIS engine

does not become negative as illustrated in simulation yields in Sect. 4. In some earlier mentioned papers, the control law also becomes negative which is not practically producible since the control law should be generated by a square of current in implementation. Superior to [27], this article considers controller design for the MEMS tunable capacitor while measurement noise is deemed in system dynamics. All the mentioned superiorities in exploitation of the MEMS VRS in this work are reliant upon the features of the controller including robustness and soft tuning of the constructive terms of the control law.

The tracking performance of the proposed PID controller and the conventional ZN PID are not so different while no measurement noise or disturbance is imposed on the system. However, Fig. 13 a and b imply a slight preference of the proposed fuzzy PID over the conventional ZN-based PID from both aspects of the tracking performance and energy consumption even at normal conditions without the measurement noise.

Fuzzy parameters will affect the performance of the controller such as percent maximum overshoot, the settling time, Integral of Absolute Error (IAE), and Integral of Squared Error (ISE). Adopting a tiny α or a tiny integral time constant T_i would yield a strong integral action. Whether the integral action should be strong or weak is determined in the scheme by comparison with the ZN PID tuning rule table. In the ZN rule, the integral time constant T_i is taken four times as large as the derivative time constant ($\alpha = 4$). α takes a value less than 4 (such as 2) to produce a stronger integral action. Consequently, the fuzzy parameters, around point a in Fig. 4a, are tuned as follows to boost integral performance of the controller:

- If e is PL and $\dot{e}$ is Z, then K_p', K_d', and α will be large, small and small, respectively.

Note that α gets equal to 2 when it becomes small. For adjustment of overshoot performance ($M_p\%$), the PID controller should have a small proportional gain to reduce the control signal. That is the reason, around point b in Fig. 4a, the fuzzy parameters are tuned as follows:

- If e is Z and $\dot{e}$ is NL, then K_p', K_d', and α will be small, large and large, respectively.

At the end, one may remark the following rules for fuzzy tuning of the parameters to adjust the performance indexes in a fuzzy PID auto-tuner:

- If the steady state error is large, then K_p' will be large.
- If the response is oscillatory, then K_d' will be large.
- If the response is sluggish, then K_p' will be large.
- If the steady state error is very large, then α will be small.
- If the overshoot is very large, then K_p' will be small.

The block diagram of the fuzzy PID auto-tuner is presented in Fig. 14. It should be considered that the fuzzy parameter K_p' can decrease the steady state error but can not make it zero on its own. It also makes the dynamic response more speedy, leading to greater bandwidth. However, it might bring about instability. The fuzzy parameter K_d' may result in more oscillatory response. The fuzzy parameter α can zero the steady state error.

5 Discussion

The MEMS TCs, which are the major elements of the VRS, should be operated near the pull-in point. In other terms, for a successful exploitation of the MEMS tunable capacitor, the movable plate should be moved towards a certain distance from the fixed plate. This required precise positioning control can be done with a Ziegler-Nichols PID controller, a pole-placement state feedback controller or

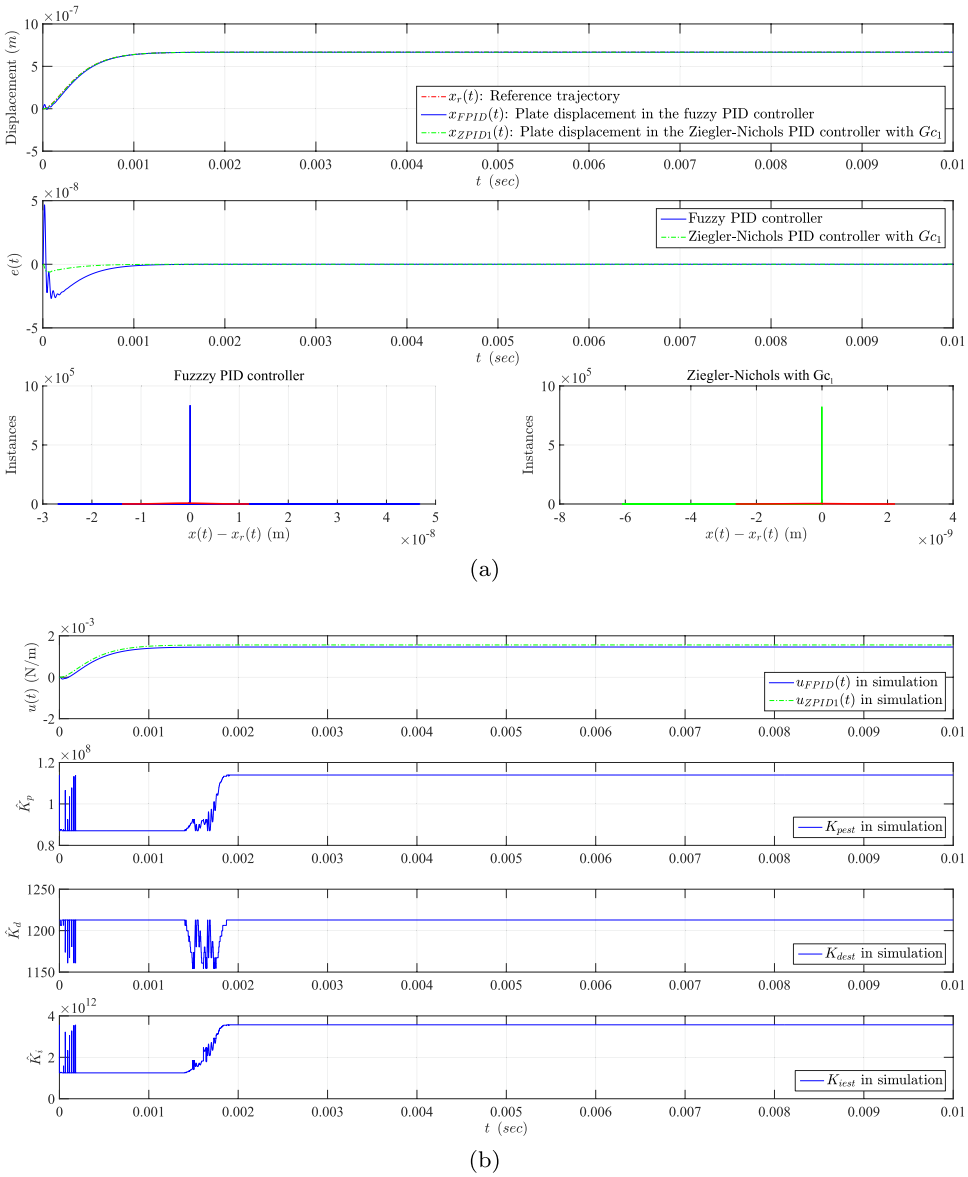

Fig. 13 Analysis of without-noise condition; **a** From top to bottom: comparison of the tracking performance between the fuzzy and ZN PIDs, comparison of the tracking error between the fuzzy and ZN PIDs, tracking error histograms of the fuzzy and ZN PIDs. **b** From top to bottom: control effort comparison between the fuzzy and ZN PIDs, and variation of the PID coefficients in the fuzzy PID system

a regulator. However, the read-out of the movable plate position state is mixed with measurement noise, making conventional PID and other plain state feedback controllers incapable of tracking the desired pull-in trajectory. The proposed fuzzy PID compensates for the misalignment of the movable plate and reduces the oscillation peaks and perturbation around the pull-in point compared with the conventional alternative controllers. Moreover, the designed fuzzy PID controller applies less control effort and consumes less energy in comparison with the ZN PID controller, while being affected by measurement noise. The last subtle point is that simulation results slightly confirm better tracking performance but this could be a life-saver if other exacerbating conditions such as uncertainty are imposed on the operational condition in addition to the measurement noise. In conclusion, it is important to

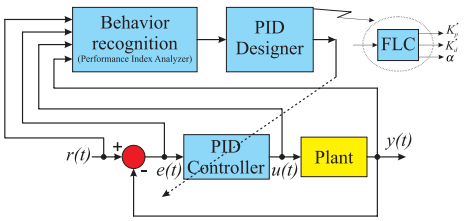

Fig. 14 The block diagram of the fuzzy PID auto-tuner

tackle the measurement noise and improve the performance even if the improvement is subtle.

From an implementation viewpoint, it is worthwhile mentioning the number of the look-up tables which each has 49 rules. This might have influence over the volume usage of the hardware memory. In implementation, the

fuzzy control is rather slow because the fuzzy controller performs numerous evaluations chiefly entailing fuzzification, inference, and defuzzification procedures for calculating the values of the control effort. It causes severe consequences in real-time application which not only requires particular hardware such as FPGA, Fuzzy logic control ASIC chip, etc., but also needs optimizations in the control loop to decrease machine cycles. Moreover, large number of tests with hardware is crucial to verify and validate the fuzzy knowledge-based rule tables.

6 Conclusion and research prospective

MEMS tunable capacitors are remarked as the chief components in AC voltage reference sources. The displaceable plate of the tunable capacitor should be driven towards the pull-in point in order to achieve the desiderated output voltage. Measurement noise of side circuits and exogenous disturbance, which are foisted upon the system dynamics, bring about problems in particular while one intends to obtain thorough faultless displacement tracking of the moveable plate towards the final pull-in point non-destructively, using either a simple pole placement controller or even a conventional MRAC. Although numerous attempts are done to plan and implement fabrication procedures to produce MEMS tunable capacitors with the desired physical properties, the uncertainties in stiffness and damping do exist in the MEMS VRS. When the mentioned malfunctioning disturbance and noise are taken into account in operation of the device, the exacerbating uncertainties are considerable. At these conditions, simple non-robust pole-placement feedback controllers are incompetent of successful drive of the MEMS device. The proposed fuzzy PID controller is competent of noise reduction in the performance of the tunable capacitor in a MEMS voltage reference source. The fuzzy soft tuning of PID coefficients make the PID controller robust against the measurement noise which is imposed on the plate displacement and velocity read-outs. This robustness brings about long-term stability of operation around the pull-in point.

One of the other issues affecting the performance of the tunable capacitor is the parameter variation. It can be considered as a research potential to modify the controller design so that it will be also robust against parameter uncertainty and modeling nonlinearities. It requires one to think over a fuzzy adaptive PID controller to cope with noise as well as parametric uncertainty. Outlining the article big picture, one problem, which requires one's prospective attention, is parameter identification in combination with the adaptive controller to calculate stiffness and damping coefficients for generation of the device catalogue information. As another future research outline, the authors are hopeful to implement the controller on a Digital Signal Processing (DSP) Integrated Circuit (IC) and evaluate the yields in practice when making attempts to code the fuzzy algorithms over reliable hardware. As last research prospectives, one may refer to a control system design while upper bounds of disturbance and parametric uncertainties are unknown. A solution might be an ASMC design established upon on Radial Basis Function (RBF) ANN for evaluation of unknown upper-bounds of lumped uncertainty and disturbance in the tunable capacitor dynamics adjacent to the pull-in point. The ANN learning system will be exploited for getting assured of stability and tracking error zero-convergence. Additionally, it is put forth as a prospective job to comparatively study performance of various powerful modern controllers, such as Linear Quadratic Gaussian controller, and the proposed fuzzy PID controller. It is worthwhile contemplating trade-off between complexities of implementation of controllers and enhancement of their performance indexes.

Declarations

Conflict of interest On behalf of all authors, the corresponding author states that there is no conflict of interest.

References

1. Abdel-Hamid W, Noureldin A, El-Sheimy N (2007) Adaptive fuzzy prediction of low-cost inertial-based positioning errors. IEEE Trans Fuzzy Syst 15(3):519–529. https://doi.org/10.1109/TFUZZ.2006.889936
2. Blard F, Bounouh A, Bélières D, Camon H (2011) Very high stability achievement in MEMS based AC voltage references. In: IEEE 24th International Conference on Micro Electro Mechanical Systems (MEMS), pp 656–659, https://doi.org/10.1109/MEMSYS.2011.5734510
3. Bounouh A, Camon H, Bélières D, Blard F, Ziadé F (2011) MEMS AC voltage reference for miniaturized instrumentation and metrology. Computer Standards and Interfaces 33(2):159–164, https://doi.org/10.1016/j.csi.2010.06.007, XVI IMEKO TC4 "Symposium Exploring New Frontiers of Instrumentation and

Methods for Electrical and Electronic Measurements" and XIII International Workshop on ADC Modelling and Testing
4. Bounouh A, Camon H, Belieres D (2012) MEMS based AC voltage references with very high stability. In: Conference on Precision Electromagnetic Measurements (CPEM), pp 552–553, https://doi.org/10.1109/CPEM.2012.6251048
5. Bounouh A, Camon H, Belieres D (2013) Wideband high stability MEMS-Based AC voltage references. IEEE Trans Instrum Measurement 62(6):1646–1651. https://doi.org/10.1109/TIM.2012.2225963
6. Castañer L, Pons J, Nadal-Guardia R, Rodrıǵuez A (2001) Analysis of the extended operation range of electrostatic actuators by current-pulse drive. Sens Actuators A: Phys 90(3):181–190. https://doi.org/10.1016/S0924-4247(01)00525-8
7. Cheng L, Yunxiangi G, Yanchi S (2018) Adaptive sliding mode control method for MEMS gyroscope using prescribed performance approach. In: 2018 37th Chinese Control Conference (CCC), pp 3102–3107, https://doi.org/10.23919/ChiCC.2018.8484062
8. Deng J, Liu C, Hao Y, Liu S, Meng F, Xu P (2016) Control method of pull-in voltage on the MEMS inertial switch integrating actuator and sensor. Microsyst Technol 23(10):4785–4795. https://doi.org/10.1007/s00542-016-3236-1
9. Dorf R, Bishop R (2016) Modern Control Systems, Global Edition. Pearson Education Limited, https://books.google.co.id/books?id=uhtwjwEACAAJ
10. Farzanegan B, Niafar E, Ranjbar E, Suratgar AA (2019) Two MRAC designs for the MEMS-Based AC voltage reference source. Iran J Sci Technol Trans Electr Eng. https://doi.org/10.1007/s40998-019-00205-7
11. Fei J (2010) Robust adaptive vibration tracking control for a micro-electro-mechanical systems vibratory gyroscope with bound estimation. IET Control Theory Appl 4(6):1019–1026. https://doi.org/10.1049/iet-cta.2008.0199
12. Fei J, Batur C (2009) A novel adaptive sliding mode control with application to MEMS gyroscope. ISA Trans 48(1):73–78. https://doi.org/10.1016/j.isatra.2008.10.008
13. Fei J, Chen F (2020) Dynamic fractional order sliding mode control method of micro gyroscope using double feedback fuzzy neural network. IEEE Access 8:125097–125108. https://doi.org/10.1109/ACCESS.2020.3007233
14. Fei J, Feng Z (2019) Adaptive fuzzy super-twisting sliding mode control for microgyroscope. Complex 2019:6942642:1-6942642:13. https://doi.org/10.1155/2019/6942642
15. Fei J, Xin M (2014) Adaptive fuzzy backstepping sliding mode control for MEMS gyroscope. J Intell Fuzzy Syst 27(2):817–826. https://doi.org/10.3233/IFS-131040
16. Fei J, Xin M, Juan W (2013) Adaptive fuzzy sliding mode control using adaptive sliding gain for MEMS gyroscope. Trans Inst Measurement Control 35(4):551–558. https://doi.org/10.1177/0142331212455451
17. Fei J, Wang Z, Liang X (2020) Robust adaptive fractional fast terminal sliding mode controller for microgyroscope. Complex 2020:8542961:1-8542961:18. https://doi.org/10.1155/2020/8542961
18. Hong SK (2008) A fuzzy logic based performance augmentation of MEMS gyroscope. J Intell Fuzzy Syst 19(6):393–398
19. Jafari M, Mobayen S, Roth H, Bayat F (2020) Nonsingular terminal sliding mode control for micro-electro-mechanical gyroscope based on disturbance observer: Linear matrix inequality approach. Journal of Vibration and Control p 1077546320988192, 10.1177/1077546320988192
20. Jeon H, Grunwald D (2005) Design of servo control systems with quadratic optimal control and observed-state feedback control for mems-based storage device. Microsyst Technol 11(08):1005–1012. https://doi.org/10.1007/s00542-005-0528-2
21. Juan W, Fei J (2013) Adaptive fuzzy approach for non-linearity compensation in MEMS gyroscope. Trans Inst Measurement Control 35(8):1008–1015. https://doi.org/10.1177/0142331212472224
22. Kärkkäinen A, Oja A, Kyynäräinen J, Kuisma H, Seppä H (2004a) Stability of electrostatic actuation of MEMS. Physica Scripta T114:193. https://doi.org/10.1088/0031-8949/2004/T114/048
23. Kärkkäinen A, Pesonen N, Suhonen M, Kyynarainen J, Oja A, Manninen A, Tisnek N, Seppa H (2004b) AC voltage reference based on a capacitive micromechanical component. In: Conference on Precision Electromagnetic Measurements Digest, pp 119–120, https://doi.org/10.1109/CPEM.2004.305489
24. Kärkkäinen AM (2006) MEMS based voltage references. PhD thesis, VTT Technical Research Centre of Finland, Vuorimiehentie 3, P.O. Box 1000, FI-02044 VTT, Finland, dissertation for the degree of Doctor of Philosophy to be presented with due permission of the Department of Electrical and Communications Engineering for public examination and debate in the Large Seminar Hall of Micronova at Helsinki University of Technology
25. Li W, Liu PX (2011) Adaptive tracking control of an MEMS gyroscope with H-infinity performance. J Control Theory Appl 9(2):237. https://doi.org/10.1007/s11768-011-9048-z
26. Mandal S, Kumar A, Chatterjee K, Kumar A, Hanumaiah N (2014) Feasibility study on the use of 2-dimensional penalized spline trajectory for smooth curve generation in precision machining. J Autom Electr Syst 25(5):576–584. https://doi.org/10.1007/s40313-014-0138-2
27. Mehrnezhad A, Suratgar A, Khatami S, Sobhiyeh S (2013) A mathematical dynamic model for static and dynamic behaviours of MEMS-based AC voltage reference source. In: 21st Iranian Conference on Electrical Engineering (ICEE), pp 1–5, https://doi.org/10.1109/IranianCEE.2013.6599714
28. Moghadam AS, Ranjbar E, Farzanegan B, Suratgar AA, Menhaj MB (2020) Observer-based sliding mode control for mems-based ac voltage reference source. In: 2020 28th Iranian Conference on Electrical Engineering (ICEE), pp 1–6, https://doi.org/10.1109/ICEE50131.2020.9260715
29. Mondal S, Mahanta C (2013) Adaptive integral higher order sliding mode controller for uncertain systems. J Control Theory Appl 11(1):61–68. https://doi.org/10.1007/s11768-013-1180-5
30. Rahmani M, Rahman M (2019a) A new adaptive fractional sliding mode control of a MEMS gyroscope. Microsyst Technol 25(9):3409–3416. https://doi.org/10.1007/s00542-018-4212-8
31. Rahmani M, Rahman M (2019b) A novel compound fast fractional integral sliding mode control and adaptive PI control of a MEMS gyroscope. Microsyst Technol 25(10):3683–3689. https://doi.org/10.1007/s00542-018-4284-5
32. Rahmani M, Rahman M, Nosonovsky M (2020) A new hybrid robust control of MEMS gyroscope. Microsyst Technol 26(3):853–860. https://doi.org/10.1007/s00542-019-04584-z
33. Ranjbar E, Suratgar AA (2020) Design of an adaptive sliding mode controller with a sliding mode luenberger observer for the MEMS capacitive plates. SN Appl Sci. https://doi.org/10.1007/s42452-020-2148-y
34. Ranjbar E, Mehrnezhad A, Suratgar AA (2017) Adaptive sliding mode control of MEMS AC voltage reference source. J Control Sci Eng. https://doi.org/10.1155/2017/9425190
35. Ranjbar E, Yaghoubi M, Suratgar AA (2019) Adaptive sliding mode controller design for a tunable capacitor susceptible to unknown upper-bounded uncertainties and disturbance. Iran J Sci Technol Trans Electr Eng. https://doi.org/10.1007/s40998-019-00220-8
36. Ranjbar E, Yaghubi M, Suratgar AA (2020) Robust adaptive sliding mode control of a mems tunable capacitor based on deadzone method. Automatika 61(4):587–601. https://doi.org/10.1080/00051144.2020.1806011

37. Huang Shiuh-Jer, Lin Wei-Cheng (2003) Adaptive fuzzy controller with sliding surface for vehicle suspension control. IEEE Trans Fuzzy Syst 11(4):550–559. https://doi.org/10.1109/TFUZZ.2003.814845
38. Sinha S, Mandal N (2019) Design of a smart pressure transmitter and its temperature compensation using artificial neural network. J Control, Autom Electr Syst 30(1):95–103. https://doi.org/10.1007/s40313-018-00430-1
39. Suhonen M, Seppa H, Oja A, Heinila M, Nakki I (1998) AC and DC voltage standards based on silicon micromechanics. In: Conference on Precision Electromagnetic Measurements Digest, pp 23–24, https://doi.org/10.1109/CPEM.1998.699739
40. Talole SE (2018) Active disturbance rejection control: Applications in aerospace. Control Theory Technol 16(4):314–323. https://doi.org/10.1007/s11768-018-8114-1
41. Wu D, Fei J (2016) Adaptive neural sliding control of MEMS gyroscope with robust feedback compensator. Trans Inst Measurement Control 38(4):414–424. https://doi.org/10.1177/0142331215585879
42. Zhao L, Luo S, Guanci Y, Dong R (2020) Chaos analysis and stability control of the MEMS resonator via the type-2 sequential FNN. Microsyst Technol. https://doi.org/10.1007/s00542-020-04935-1
43. Zhao Zhen-Yu, Tomizuka M, Isaka S (1993) Fuzzy gain scheduling of PID controllers. IEEE Trans Syst Man Cybern 23(5):1392–1398. https://doi.org/10.1109/21.260670